Spatiotemporal dynamics of ecosystem fires and biomass burning-induced carbon emissions in China over the past two decades

Anping Chen, Rongyun Tang, Jiafu Mao, Chao Yue, Xiran Li, Mengdi Gao, Xiaoying Shi, Mingzhou Jin, Daniel Ricciuto, Sam Rabin, et al.

Geography and Sustainability 1 (2020) 47–58

Contents lists available at ScienceDirect

Geography and Sustainability

journal homepage: www.elsevier.com/locate/geosus

Article

Spatiotemporal dynamics of ecosystem fires and biomass burning-induced carbon emissions in China over the past two decades

Anping Chen[a,b,*], Rongyun Tang[c,d], Jiafu Mao[d,*], Chao Yue[e], Xiran Li[a,f], Mengdi Gao[g], Xiaoying Shi[d], Mingzhou Jin[c], Daniel Ricciuto[d], Sam Rabin[h], Phillippe Ciais[i], Shilong Piao[g]

[a] Department of Biology, Colorado State University, Fort Collins, CO 80523, USA
[b] Graduate Degree Program in Ecology, Colorado State University, Fort Collins, CO 80523, USA
[c] Department of Industrial and Systems Engineering, University of Tennessee, Knoxville, TN 37996, USA
[d] Environmental Sciences Division and Climate Change Science Institute, Oak Ridge National Laboratory, Oak Ridge, TN 37831, USA
[e] State Key Laboratory of Soil Erosion and Dryland Farming on the Loess Plateau, Northwest Agriculture & Forestry University, Yangling, Shanxi 712100, China
[f] College of Urban and Environmental Sciences, Central China Normal University, Wuhan, Hubei 430079, China
[g] Sino-French Institute for Earth System Science, College of Urban and Environmental Sciences, Peking University, Beijing 100871, China
[h] Atmospheric Environmental Research (IMK-IFU), Institute of Meteorology and Climate Research, Karlsruhe Institute of Technology (KIT), Kreuzeckbahnstraße 19, Garmisch-Partenkirchen 82467, Germany
[i] LSCE, UMR CEA-CNRS, Bat. 709, CE, L'Orme des Merisiers, Gif-sur-Yvette 91191, France

HIGHLIGHTS

- Ecosystem fire in China was investigated with satellite data and model simulations
- We found large discrepancy in fire data between different approaches
- Burned area and C emissions were high in boreal forest and subtropical dry forest
- Climate and human factors dominated the spatial and seasonal fire patterns

GRAPHICAL ABSTRACT

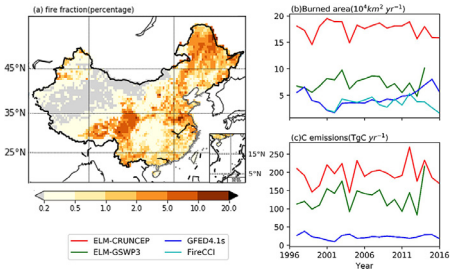

ARTICLE INFO

Article history:
Received 30 January 2020
Received in revised form 21 February 2020
Accepted 23 February 2020
Available online 9 March 2020

Keywords:
Fire emission
Burned area
Fire models
China

ABSTRACT

Fire is a major type of disturbance that has important influences on ecosystem dynamics and carbon cycles. Yet our understanding of ecosystem fires and their carbon cycle consequences is still limited, largely due to the difficulty of large-scale fire monitoring and the complex interactions between fire, vegetation, climate, and anthropogenic factors. Here, using data from satellite-derived fire observations and ecosystem model simulations, we performed a comprehensive investigation of the spatial and temporal dynamics of China's ecosystem fire disturbances and their carbon emissions over the past two decades (1997–2016). Satellite-derived results showed that on average about 3.47 - 4.53 × 10^4 km^2 of the land was burned annually during the past two decades, among which annual burned forest area was about 0.81 - 1.25 × 10^4 km^2, accounting for 0.33-0.51% of the forest area in China. Biomass burning emitted about 23.02 TgC per year. Compared to satellite products, simulations from the Energy Exascale Earth System Land Model (ELM) strongly overestimated China's burned area and fire-induced carbon emissions. Annual burned area and fire-induced carbon emissions were high for boreal forest in Northeast China's Daxing'anling region and subtropical dry forest in South Yunnan, as revealed by both the satellite product and the model simulations. Our results suggest that climate and anthropogenic factors play critical roles in controlling the spatial and seasonal distribution of China's ecosystem fire disturbances. Our findings highlight the importance of multiple complementary approaches in assessing ecosystem fire disturbance and its carbon consequences. Further studies are required to improve the methods of observing and modelling China's ecosystem fire disturbances, which will provide valuable information for fire management and ecosystem sustainability in an era when both human activities and the natural environment are rapidly changing.

* Corresponding authors.
E-mail addresses: anping.chen@colostate.edu (A. Chen), maoj@ornl.gov (J. Mao).

https://doi.org/10.1016/j.geosus.2020.03.002

1. Introduction

Fire is a major type of disturbance that is widely observed in almost every terrestrial biome (Archibald et al., 2010; Bowman et al., 2009; De Groot et al., 2013; Kaye et al., 2010; Williams et al., 2009). Globally, it is estimated that about 345–464 Mha is burned every year (Giglio et al., 2013; Randerson et al., 2012) for the satellite observation period (1990s–2000s), resulting in a total carbon emission of 1.9-2.5 Pg C yr^{-1} (Randerson et al., 2012; van der Werf et al., 2010; Van Der Werf et al., 2017), which is equivalent to 4% of global terrestrial net primary productivity (NPP) (van der Werf et al., 2006; Zhao and Running, 2010). In many biomes, fire disturbances also play a critical functional role in determining vegetation distribution and successional dynamics (Barrett et al., 2011; Feurdean et al., 2017; Staver et al., 2011; Wirth et al., 2008; Zeng et al., 2014). For instance, fire disturbance and its roles in forest ecosystem functioning and carbon dynamics have been extensively studied for boreal forest (Beck et al., 2011; Bond-Lamberty et al., 2007; Chu & Guo, 2014; French et al., 2011; Liu et al., 2019; Stinson et al., 2011), tropical and subtropical forest (Cochrane et al., 1999; Hoffmann et al., 2012; Lehmann et al., 2014), and Mediterranean chaparral (Pausas and Fernández-Muñoz, 2012; Weise et al., 2017). In temperate Asia especially including China, however, ecosystem fires and their impacts remain under-investigated. Efforts to quantify burned area and related carbon dynamics usually result in large uncertainties (Knorr et al., 2012; Veraverbeke et al., 2015). With the ongoing rapid changes of the climate and biosphere, there is an urgent need for a better quantification of fire disturbances and their impacts on regional and global carbon cycles (Adab et al., 2018; Konovalov et al., 2014; Shvidenko et al., 2011).

Recent advances in remote sensing and fire modelling, along with the accumulation of global observation data in climate, vegetation, and fire, greatly expand our capacity in understanding fire disturbance and fire carbon dynamics over a broad geographical range (Abatzoglou et al., 2018; Archibald et al., 2013; Hantson et al., 2016; Le Page et al., 2010; Migliavacca et al., 2013). In particular, the improved algorithms used to extract fire information from satellite imagery and the development of process-based fire models offer useful analytic tools for exploring fire disturbances from local to global scales (Hislop et al., 2020; Kantzas et al., 2015). Satellite derived fire products (e.g. Giglio et al., 2010; Wooster et al., 2003) provide continuous and objective monitoring of fire disturbances over a broad geographical range, and have been widely used in model benchmarking and data intercomparison (Li et al., 2012; Mouillot et al., 2014; Prentice et al., 2011; Sá et al., 2017), characterizing fire regimes (Archibald et al., 2013; Chen et al., 2017), and estimating regional and global fire carbon emissions (Kaiser et al., 2012; Konovalov et al., 2014; Li et al., 2013; Van Der Werf et al., 2017). However, the accuracy of those satellite derived products is subject to the spatial resolution of satellite imagery, as well as the performance of the fire detection algorithms (Kumar et al., 2018; Randerson et al., 2012; Roy and Boschetti, 2009). Furthermore, satellite fire products do not provide mechanistic understanding of fire disturbances, and thus cannot be used to predict the changes in fire regimes under projected future climate and anthropogenic schemes. Although scientists have long hoped to statistically define fire disturbances from climate, just like vegetation (Archibald et al., 2013; Veraverbeke et al., 2015), the relationship between climate and fire has been suggested as nonlinear and can be greatly modified by the complex interactions and feedbacks among climate, vegetation, anthropogenic activities, and fire (Archibald et al., 2009; Field et al., 2016; Knorr et al., 2013; Malamud et al., 1998; Syphard et al., 2017). Process-based fire modelling provides a new avenue to explore the spatio-temporal dynamics of fire disturbance and the underlying mechanisms (Hoffman et al., 2018; Kloster et al., 2012; Yang et al., 2014a). Yet as fire disturbance is a complicated process influenced by many natural and anthropogenic factors, current models still need more fine tuning and calibration against observation data (Migliavacca et al., 2013; Syphard et al., 2017; Yue et al., 2014). A combined approach that integrates observation and modelling, therefore, could be especially helpful in examining and comprehending the extent of fire disturbances and their impacts on carbon cycles across the space and time.

Here, we take advantage of the recent advances in satellite-derived fire data, combined with an ecosystem simulation model, the state-of-the-art Energy Exascale Earth System Land Model (ELM), to investigate the spatial distribution and temporal dynamics of ecosystem fire disturbance and its carbon emissions in China over the period of 2000-2016. Located mostly in the northern temperate region, China occupies a broad geographical range and has very diverse ecosystems. Ecosystem fire disturbances thus vary greatly in intensity and frequency across its broad geographical range (Zhong et al., 2003). For example, the crop fires in central and southeast China are well-controlled anthropogenic biomass burning, frequently occurring after harvest. Grassland fires in Inner Mongolia are mainly limited by climate but are also heavily suppressed by humans and thus come with a lower frequency (Guo et al., 2003; Liu and Zhang, 2019). Forest fires, the prevention of which is strongly required by the government (Oliveira et al., 2017; Yan et al., 2006), are under strict control and intensive monitoring by the forestry administration agency. Recreational and agricultural uses of fire are among the most common causes of forest fires (Ying et al., 2018). Boreal forest in Northeast China and subtropical dry forests in South Yunnan are typically fire-prone ecosystems (Han et al., 2015; Kasischke and Turetsky, 2006; Van der Werf et al., 2008; Wilgen et al., 1985). For instance, a severe fire in Northeast China's Daxing'anling region in 1987 burned about 1.3 million hectares (Mha) of forest, which is the recorded largest forest fire in China (Cahoon et al., 1994).

Given China's dense population and highly fragmented landscape patches, ecosystem fires could impose significant threats to ecosystem sustainability and the safety of the society (Zhang et al., 2019; Zhong et al., 2003). On the other hand, human activities could profoundly alter fire regimes (Miao et al., 2017; Tao et al., 2013). Several studies have started to assess the characteristics of ecosystem fires and their impact on carbon cycles, especially the northeastern boreal forests (Huang et al., 2018; Tian et al., 2011; Wang et al., 2001). However, results vary greatly in those assessments, largely due to their differences in data sources and methods (Lü et al., 2006; Song et al., 2009; Yan et al., 2006; Ying et al., 2018). Moreover, even less is known about temporal dynamics of China's ecosystem fires and associated carbon emissions, which are critical for fire and ecosystem management, as well as the modelling and prediction of forest carbon cycles. Hence, specific goals of this study include: (1) to identify places with a high risk of fire disturbances, (2) to understand changes of forest fire burned area and carbon emissions over the past two decades, and (3) to compare burning and carbon emission data from different approaches.

2. Data and Methods

2.1. Satellite derived burned area and carbon emissions

Two types of satellite fire products were used in this study, including the burned area data of GFED4.1s and associated fire carbon emissions data by CASA (Carnegie-Ames-Stanford-Approach) model (Randerson et al., 2012; Van Der Werf et al., 2017; https://doi.org/10.3334/ORNLDAAC/1293), and the Fire_CCI v5.1(burned area only) by the European Space Agency (Chuvieco et al., 2018; Lizundia-Loiola et al., 2020). The GFED4.1s monthly burned area data were generated from MODIS (MODerate-resolution Imaging Spectroradiometer) satellite imagery, with supplementary images from the TRMM VIRS and ERS ATSR images (Randerson et al., 2012; Randerson et al., 2017). The dataset covers the globe since 1997 at a resolution of 0.5° by 0.5°. The burned area at each 0.5° by 0.5° grid cell was partitioned into different land cover types by using the

MOD12Q1 land cover map (Friedl et al., 2010). Fire carbon emissions in GFED4.1s were simulated by the CASA biosphere model as forced by the GFED4.1s burned area (Van Der Werf et al., 2017). Small fires in GFED4.1s were statistically derived from MODIS-based burned area and active fire detections (Randerson et al., 2012; Van Der Werf et al., 2017).

Fire_CCI v5.1 was developed by the European Space Agency's (ESA)'s Climate Change Initiative (CCI) programme, and was mainly based on MOD09GQ Collection 6 images of 250 m spatial resolution (Chuvieco et al., 2018). Burned area in Fire_CCI v5.1 was generated from the red and near-infrared reflectance and thermal anomaly information of the MODIS sensor (Chuvieco et al., 2018; Lizundia-Loiola et al., 2020). Gridded data by Fire_CCI v5.1 was at the 0.25° by 0.25° resolution and covered the global ecosystems from 2001 to the present. Here we used biweekly burned area data for the period of 2001-2016. The dataset is known to have higher omission errors for the burned areas than commission errors for the unburned areas (Chuvieco et al., 2018).

2.2. Model simulated burned area and carbon emissions

The ELM version 1.0 was used to conduct the single-factor simulations of fire-induced burned area and carbon emission. Based on the Community Land Model Version 4.5 (CLM4.5), ELM has made remarkable improvements and evaluations on the land carbon and nutrient interactions (Metcalfe et al., 2017; Yang et al., 2014b) as well as hydrology changes (Forbes et al., 2019; Shi et al., 2015). The default ELM fire model, CLM-Li (Li et al., 2013), was utilized to characterize the fire response and feedback to other ELM components. The CLM-Li contains four sub-modules including non-peat fires, agricultural fires, deforestation fires, and peat fires. For non-peat fires, grid-cell level burned area is a process-based function of fire counts and sizes with the constraint of climate, soil conditions, vegetation characteristics and human suppression (e.g. population density). The fire constraints, however, are quite different for the other three empirical fire components. For example, agriculture fires are determined by cropland fraction, socioeconomic factors, and historical crop fire timing; deforestation fires depend on the deforestation intensity caused by land use and climate conditions; while peat fires are dependent on the peat fraction and water table. Fire related carbon emissions are converted from the simulated burned area, plant functional type (PFT)-based combustion completeness, and fuel loads derived from the carbon pools of leaves, stems, and aboveground litter.

Two sets of ELM semi-factorial simulations were conducted at 0.5° by 0.5° spatial resolution, separately driven by the climates of CRUNCEP version 8 (1901-2016) and GSWP3 version 1 (1901-2014) (Van Den Hurk et al. 2016). Other external forcings (e.g., the CO_2 concentration, nitrogen deposition, land use and land cover change) were also activated and detailed by (Forbes et al., 2018; Forbes et al., 2019). To disentangle the individual effects of different climate and anthropogenic factors on the studied fire variables, six sensitivity simulations using each set of the abovementioned climate driver were performed. Similar to previous work (Huntzinger, 2013; Mao et al., 2015), each ELM run consists of a spin-up period and the controlled historical simulations. The spin-up states were achieved by cycling the climate data, either CRUNCEP or GSWP, from 1901 to 1915, but other environmental drivers (e.g, the CO_2 concentration) stayed constant at 1850 level. In addition, we also conducted 5 semi-factorial simulations between 1850 and 2016 for the CRUNCEP and 1850-2014 for the GSWP (totally 10 for two-set simulations), in which each simulation included one time-varying driver while others remained unchanged. By computing the differences among selected simulations, we were able to examine the impacts of climate change, land use and land cover change, atmospheric CO_2, nitrogen deposition, aerosol deposition, and total anthropogenic activities on the interested fire activities.

3. Results

3.1. Annual burned area and fire-induced carbon emissions in China

As shown in Fig. 1a and Table 1, China's annual burned area estimated from GFED4.1s ranged between 1.76×10^4 km^2 and 8.04×10^4 km^2 during 1997–2016, with an average of 4.53×10^4 km^2 (± 1 SD = 1.51×10^4 km^2). Similarly, burned area derived from Fire_CCI v5.1 was between 1.64 and 5.33×10^4 km^2 with an average of 3.47×10^4 km^2. By dividing the land ecosystem into forest, grassland, and cropland (Hou, 2019), we showed that the average annual burned forest area derived from the satellite products was about 0.81 - 1.25 $\times 10^4$ km^2, accounting for 23.4-27.7 % of the total burned area or 0.33-0.51% of China's total forest coverage (Fig. 2). For grassland, satellite-derived annual burned area was about 1.39-1.99 $\times 10^4$ km^2 (Fig. 2). Satellite derived ecosystem burned area showed considerable inter-annual variations (Fig. 1a). For GFED4.1s, we found an increasing trend of 0.125×10^4 km^2 yr^{-1} (r=0.48, P=0.03) over 1997-2016. However, there was no significant temporal trend for burned area derived from Fire_CCI v5.1 during the whole study period (r=0.005, P=0.99). Lizundia-Loiola et al. (2020) indicated that MODIS-based burned area could be underestimated prior to July 2002 due to the availability of a single satellite. We thus also used 2003-2016 for inter-annual burned area trend analyses, which showed contrasting trends for GFED4.1s and Fire_CCI v5.1—burned area increased at a rate of 0.285×10^4 km^2 yr^{-1} for GFED4.1s (r=0.86, P=9.6×10^{-5}) but showed no trend for Fire_CCI v5.1 (r= −0.45, P=0.11) during 2003-2016. It also appeared that the two datasets showed divergent trends since ca. 2012 (Fig. 1a), likely due to the inclusion of small fires in recent GFED4.1s but not in Fire_CCI v5.1. For Fire_CCI v5.1, burned area seemed to remain relatively stable before 2010, but to increase since 2010 (Fig. 1a). However, due to the short length of the period, it is unclear if the change since 2010 in Fire_CCI v5.1 represents a real long-term trend or just some inter-annual variations.

ELM driven by GSWP3 climate data was able to reproduce the annual total burned area estimated by satellite products (Fig. 1a and Table 1). ELM-GSWP3 estimated burned area was about 7.54×10^4 km^2 (range: 4.84 - 10.13 $\times 10^4$ km^2) during 1997–2016, higher than that from satellite products. However, ELM driven by CRUNCEP climate data notably overestimated China's ecosystem burned area by an average factor of 2.66 compared to satellite fire products (Fig. 1a and Table 1). According to ELM-CRUNCEP simulations, China's ecosystem burned area over 1997-2016 was between 14.91 and 18.91×10^4 km^2. The difference between two ELM simulations driven by different climate datasets may arise from their difference in key variables, for instance, the relative humidity (RH2M) and air temperature (TSA), that modulate simulated fire activities (Supplementary Fig. S1). For both ELM-GSWP3 and ELM-CRUNCEP simulations, there was no trend in annual burned area (r=0.10, P=0.70 for ELM-GSWP3; and r=-0.15, P=0.31 for ELM-CRUNCEP). This lack of inter-annual changing trend of burned area was also found for the period after 2003 (r=-0.23, P=0.45 for ELM-GSWP3; and r=-0.29, P=0.31 for ELM-CRUNCEP).

Fire-induced ecosystem carbon emissions estimated by GFED4.1s ranged between 9.53 TgC yr^{-1} and 38.18 TgC yr^{-1} over the period of 1997–2016, with a mean value of 23.02 TgC yr^{-1} (Fig. 1b, Table 1). In addition, ecosystem fire carbon emission by GFED4.1s showed no significant trend during either 1997–2016 (r=-0.06, P=0.79) or 2003-2016 (r=-0.12, P=0.68). On the other hand, ELM model-simulated ecosystem fire carbon emissions for ELM-GSWP3 ranged between 83.35 TgC yr^{-1} and 216.28 TgC yr^{-1} during 1997–2014, with a mean rate of 131.09 TgC yr^{-1}; and for ELM-CRUNCEP between 141.61 TgC yr^{-1} and 269.14 TgC yr^{-1} during 1997–2016, with a mean rate of 177.82 TgC yr^{-1} (Table 1). Both model-simulated fire carbon emissions were much higher than those from GFED4.1s but, like the latter, showed no trend during the study period (Fig. 1b).

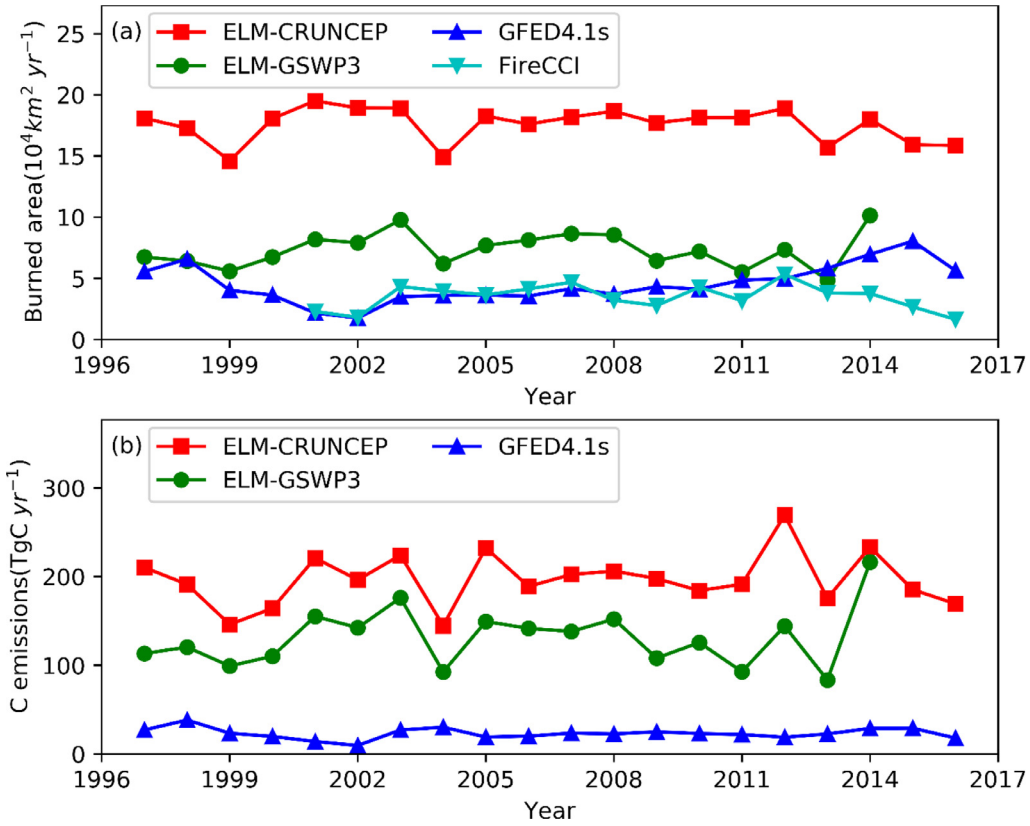

Fig. 1. (a) Annual burned area estimated from different approaches; (b) annual ecosystem fire induced carbon emissions.

Table 1
The burned area and carbon emissions of ecosystem fires in China from different sources.

Source	Period	Burned Area ($km^2\ yr^{-1}$)	Emissions ($TgC\ yr^{-1}$)	Citation
L3JRC (remote sensing)	2001–2006	93,175	37.5	Song et al., 2009
MCD45A1 (remote sensing)	2001–2006	4,175	0.8	Song et al., 2009
Gov. statistics	1980–1989	3,110	4.9	Lü et al., 2006
Gov. statistics	1990–1999	403	0.7	Lü et al., 2006
Gov. statistics	1998–2002	541	1.1	Yan et al., 2006
GBA2000 (remote sensing)	2000	21,457	25.4	Yan et al., 2006
GFED4.1s (remote sensing)	1997-2016	45,292	23.02	This study
Fire_CCI v5.1 (remote sensing)	2001-2016	34,696	-	This study
ELM model[1]	1997–2016	175,624	196.60	This study
ELM model[2]	1997–2014	73,352	131.09	This study

[1] driven by CRUNCEP climate data (https://vesg.ipsl.upmc.fr/thredds/catalog/work/p529viov/cruncep/V8_1901_2016/catalog.html).
[2] driven by GSWP3 climate data (http://cola.gmu.edu/gswp/data.html).

3.2. The spatio-temporal distribution of burned area and carbon emissions

The spatial distribution of mean annual ecosystem burned area and fire carbon emissions was highly heterogeneous (Fig. 3). Model and satellite observations differed considerably in detected ecosystem fire hotspots. Both GFED4.1s and Fire_CCI v5.1 data indicated Daxing'anling region (forest-dominated), northeast Xiaoxing'anling (forest-dominated), and Huai River Basin (agriculture-dominated) as regions of high burned area (Figs. 3e and g). In addition, East China and South China were also observed with high burned area fraction according to GFED4.1s (Fig. 3e). The spatial pattern of GFED4.1s based carbon emissions, however, did not resemble that of burned area. Fire emission hotspots were found in northeast Daxing'anling and southern Yunnan (Fig. 3f). Satellite-derived ecosystem fire hotspots in Daxing'anling, Xiaoxing'anling, and Yunnan were also reproduced by the ELM model under both CRUNCEP and GSWP3 climate forcing (Figs. 3a and c). However, the model, especially when driven with CRUNCEP climate, strongly overestimated burned area in east and southeast Qinghai-Tibetan Plateau and Mt. Changbai (Figs. 3a and c) compared to the result from satellite data. In contrast, for the Huai River Basin, model simulated burned areas were lower compared to the GFED4.1s product. For model simulations, the hotspots of ecosystem fire carbon emissions (Figs. 3b and d) were similar to that of the burned forest area (Figs. 3a and c).

Figs. 4-6 showed the spatial distribution of burned area and carbon emissions over the first and second ten years of 1997-2016 and the difference between the two sub-periods as revealed by GFED4.1s and simulated by ELM. For satellite data, there was a large increase in ecosystem fire burned area from 1997-2006 to 2007-2016 over central Northeast China and East China, followed by eastern Sichuan and some

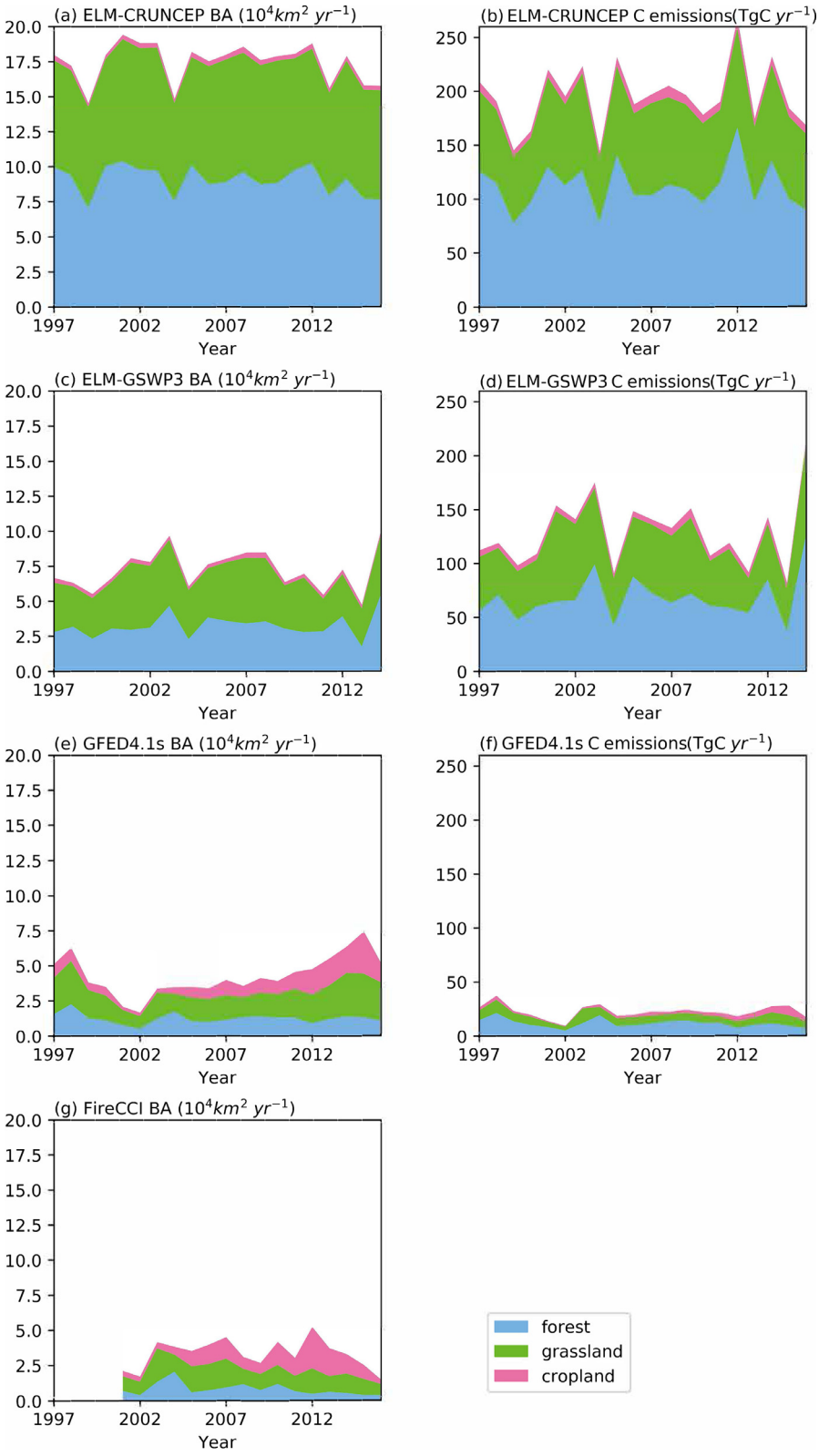

Fig. 2. Annual burned area and carbon emissions by different ecosystem types. Here we considered forest, grassland, and cropland, for which the spatial distribution information was obtained from the 1:1,000,000 vegetation map of China (Hou, 2019).

places in the Loess Plateau (Fig. 4c). Nonetheless, changes in fire carbon emissions were relatively small across most of the country, except a few scattered spots (Fig. 4f).

On the other hand, the large increase in burned area in East China from satellite data was not reproduced by ELM model simulations under either CRUNCEP or GSWP3 climate forcing (Figs. 5 and 6). In contrast, large increases in burned area by ELM-CRUNCEP simulations were mostly found in mid Daxing'anling, northeastern Qinghai, western Sichuan, and western and southern Yunnan (Fig. 5c). For ELM-GSWP3 simulations, we found considerable increase of burned area in

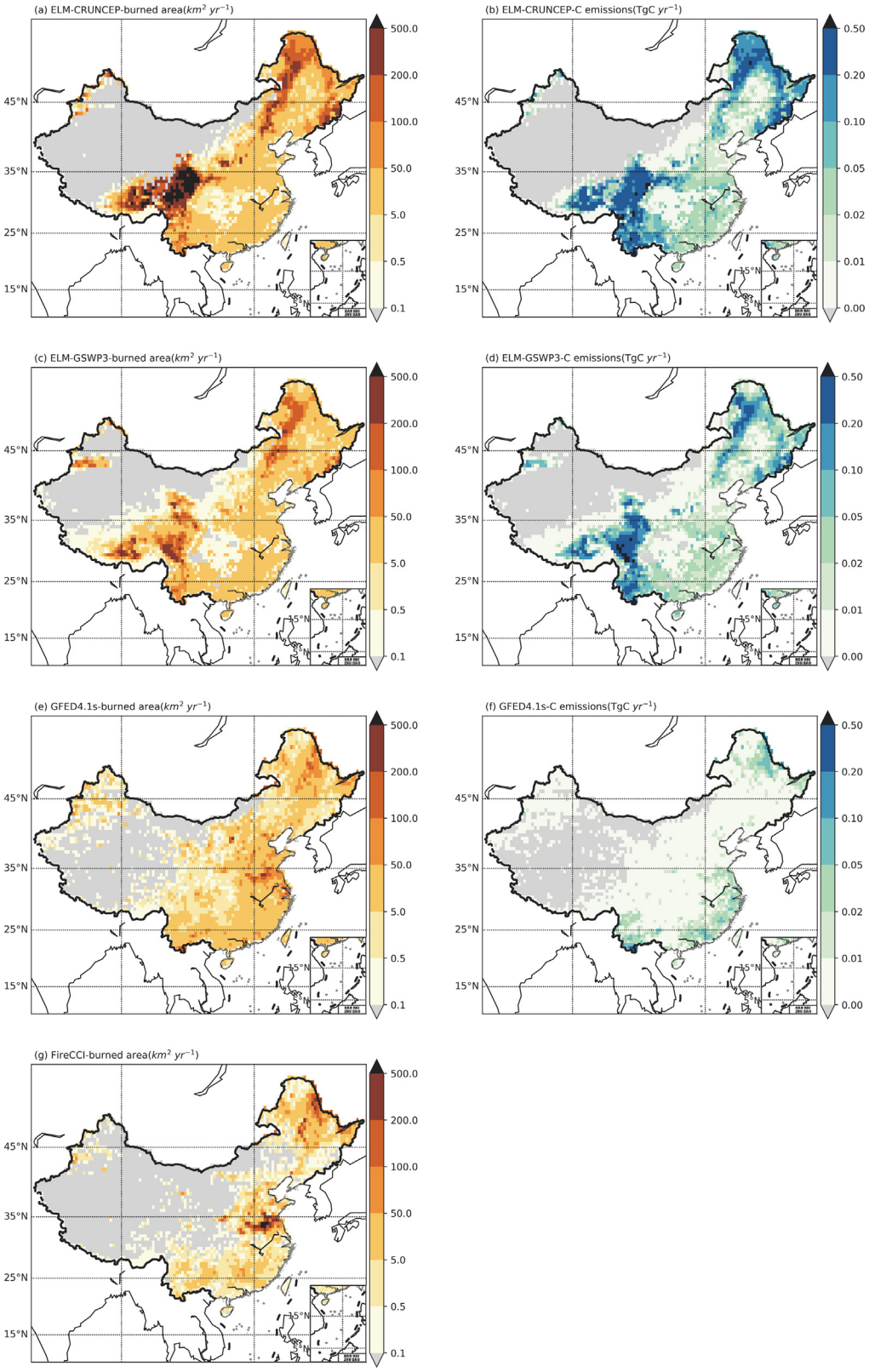

Fig. 3. The spatial distribution of mean annual burned area (a, c, e, g) and fire induced carbon emissions (b, d, f) during 1997–2016 estimated from the ELM model under the CRUNCEP (a, b) and GSWP3 (c, d) climate forcings, the GFED4.1s (e, f) and Fire_CCI v5.1 (g) satellite products. Note the spatial resolution of all the figures was 0.5 degree.

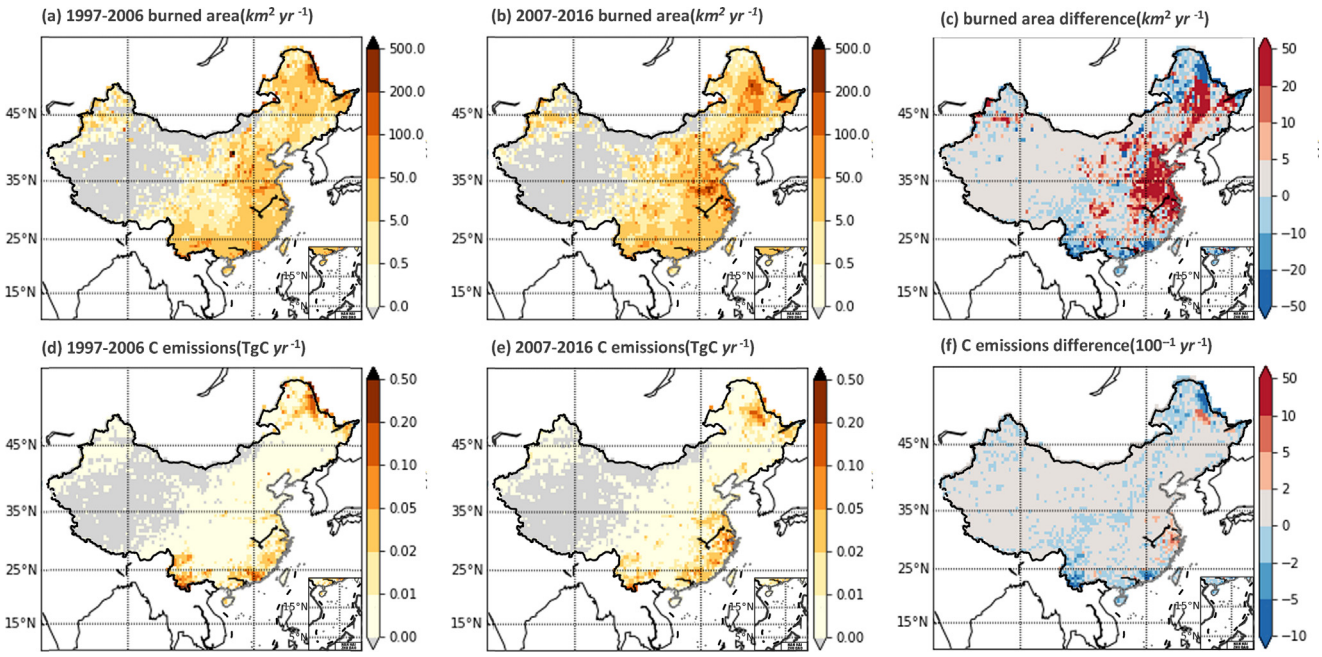

Fig. 4. The spatial distribution of mean annual burned area and carbon emissions during different time periods and the differences between the two periods, acquired from the GFED4.1s satellite data. (a–c) The spatial distribution of mean annual burned area during the first (1997-2006) and last (2007-2016) ten years, and the difference between them; (d–f) the spatial distribution of mean annual carbon emissions during the first (1997-2006) and last (2007-2016) ten years, and the difference between them.

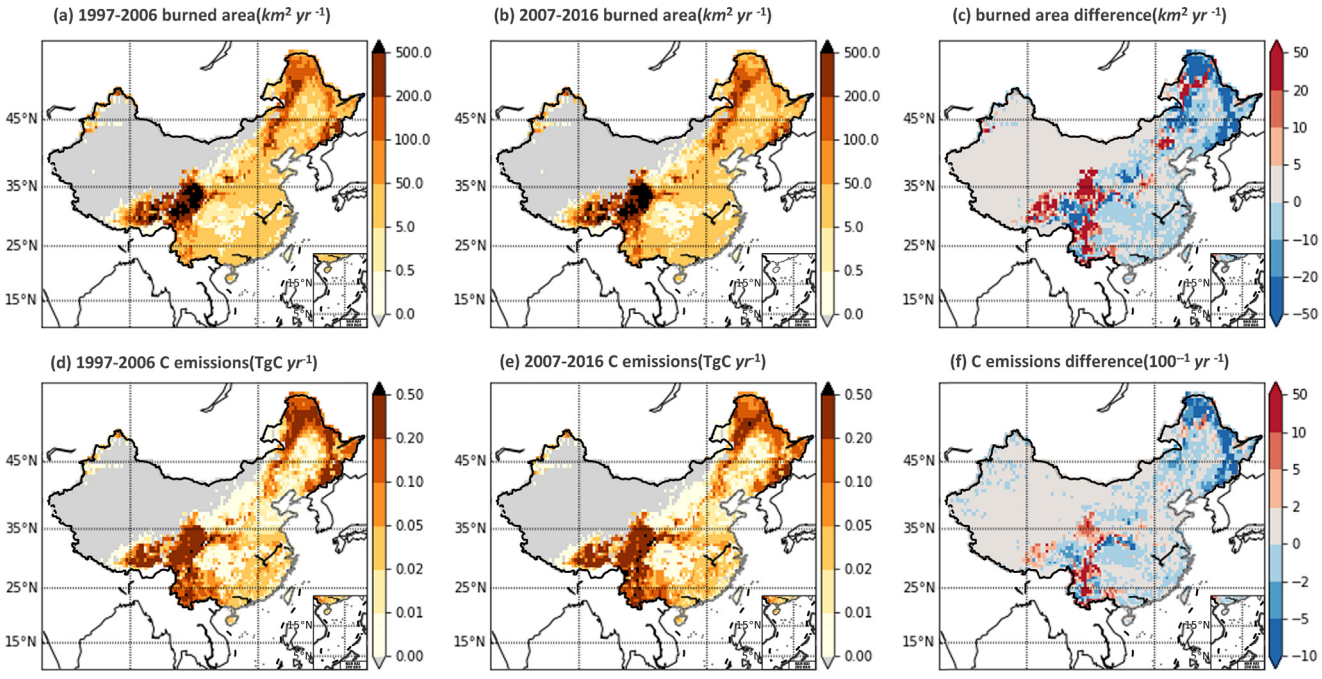

Fig. 5. The spatial distribution of mean annual burned area and carbon emissions during different time periods and the differences between the two periods, acquired from the ELM model simulations under the CRUNCEP climate forcings. (a–c) The spatial distribution of mean annual burned area during the first (1997-2006) and last (2007-2016) ten years, and the difference between them; (d–f) the spatial distribution of mean annual carbon emissions during the first (1997-2006) and last (2007-2016) ten years, and the difference between them.

Mt. Changbai, southeastern Qinghai-Tibetan Plateau, and some places of Tien Shan (Fig. 6c). Some regions also showed strong decreases in model simulated burned area, mostly in northern Daxing'anling and Xiaoxing'anling by ELM-CRUNCEP, and Daxing'anling by ELM-GSWP3 (Figs. 5c and 6c). Similarly, large changes (increases or decreases) in model-simulated fire carbon emissions also concentrated in Northeast China, southeastern Qinghai-Tibetan Plateau, and western Sichuan and Yunnan (Figs. 5f and 6f).

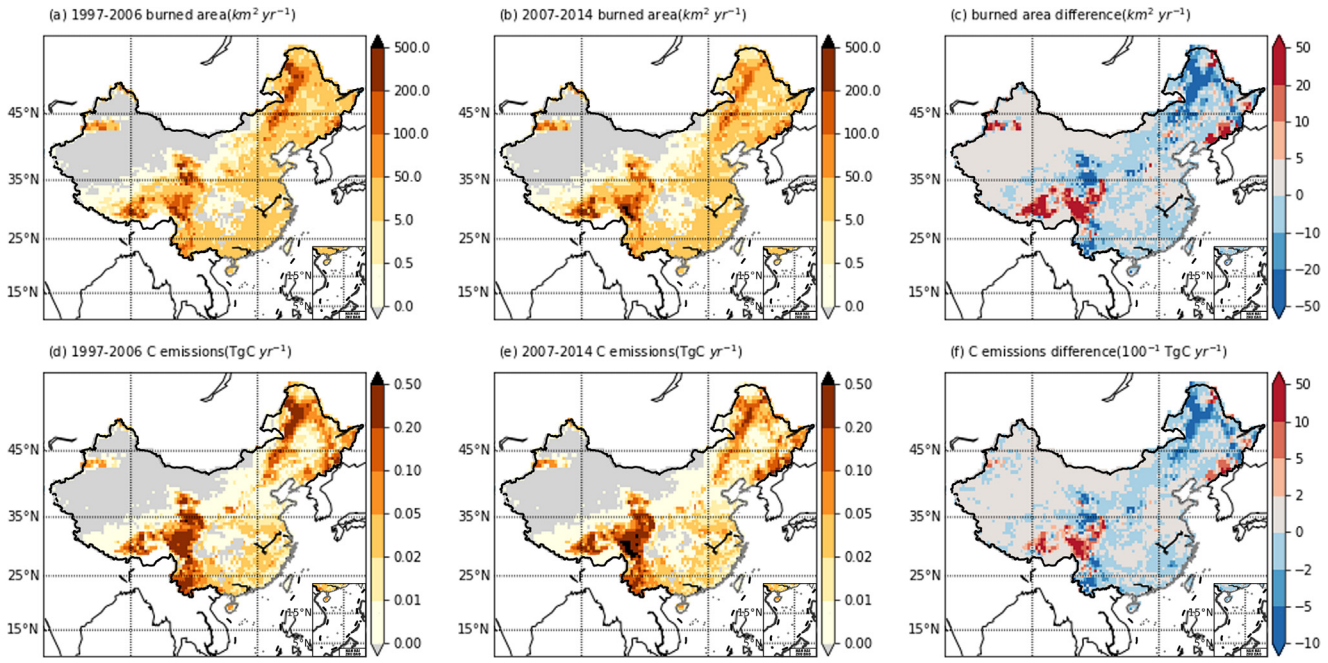

Fig. 6. The spatial distribution of mean annual burned area and carbon emissions during different time periods and the differences between the two periods, acquired from the ELM model simulations under the GSWP3 climate forcings. (a–c) The spatial distribution of mean annual burned area during 1997-2006 and 2007-2014, and the difference between them; (d–f) the spatial distribution of mean annual carbon emissions during 1997-2006 and 2007-2014, and the difference between them.

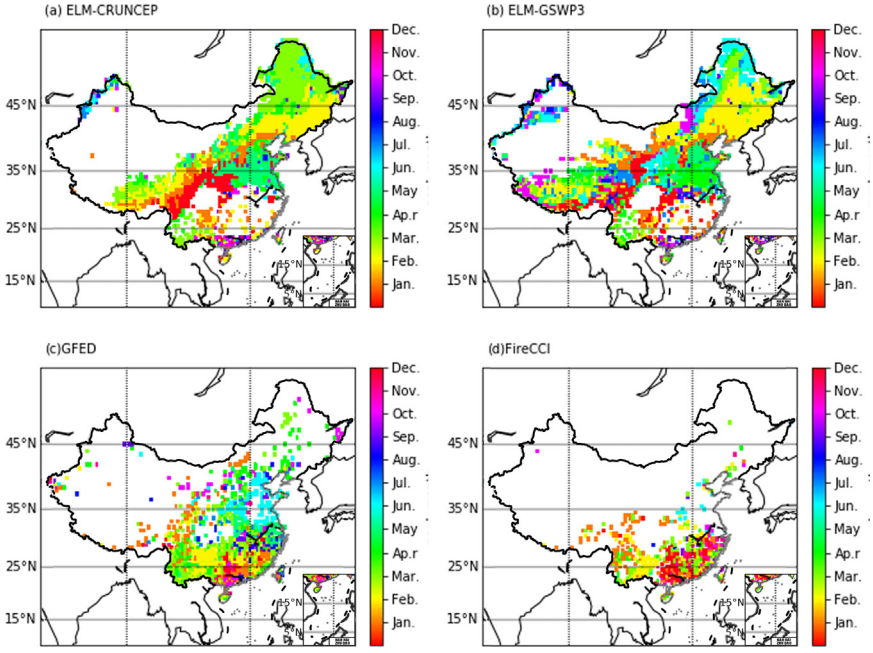

Fig. 7. The spatial distribution of month of peak burned area over the period 1997–2016 by (a) ELM-CRUNCEP, (b) ELM-GSWP3, (c) GFED4.1s, and (d) Fire_CCI v5.1.

3.3. Fire seasonality

The seasonal distribution of fire disturbance is also uneven across the country. For example, as shown in Fig. 7, the peak fire month (defined as the month with the maximum burned area) observed by GFED4.1s usually occurred in spring in Yunnan, late summer to early autumn in the Northern China Plains and western Daxing'anling, and winter in South China (Fig. 7c). Similar but much more scattered seasonal patterns were also found in Fire_CCI v5.1 satellite data (Fig. 7d). There existed clear discrepancy between the peak months derived from the satellite products and ELM model simulations, and among model simulations driven by different climate forcing datasets (Fig. 7). For example, in the Northern China Plains, satellite data suggested a peak fire month mostly in late summer to early autumn, but model simulations tended to indicate a spring peak (Fig. 7).

3.4. Drivers for model simulated fires

Results from semi-factorial simulations suggested that climate was the dominant factor responsible for model simulated temporal variations in the anomaly of fire burned area (Fig. 8). The contribution of other factors to the burned area anomaly was relatively stable across the years, with CO_2 effect, nitrogen deposition, and other anthropogenic factors leading to positive anomalies, with land use and land cover change leading to negative anomalies, for both ELM-CRUNCEP and ELM-GSWP3 simulations (Fig. 8).

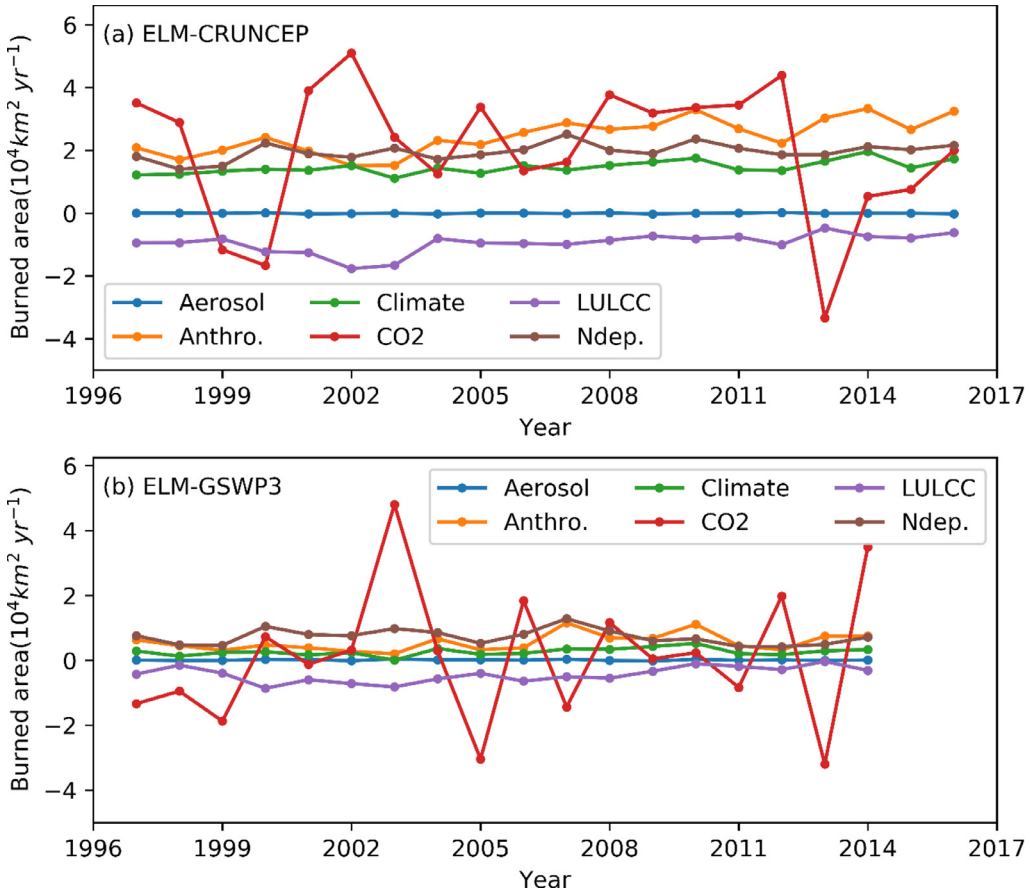

Fig. 8. Anomalies in ELM-simulated burned area in semi-factorial simulation experiments. Six factors are considered here: Aerosol, Climate, Land Use and Land Cover Change (LULCC), Anthropogenic activities other than LULCC (Anthro.), Carbon Dioxide (CO_2), and Nitrogen deposition (Ndep.)

4. Discussion

Fire disturbance is an important ecological process and has significant implications for terrestrial ecosystem carbon cycles (Bond-Lamberty et al., 2007; Pellegrini et al., 2018; Prentice et al., 2011; Yuan et al., 2012). Using data from satellite derived fire products and model simulations, we systematically assessed China's ecosystem fire burned area and associated carbon emissions over the past two decades. Observation data from satellite fire products suggest mean annual burned area was about 3.47 - 4.53 × 10^4 km^2. The discrepancy on burned area between the two satellite products may be largely attributed to the inclusion of small fires in GFED4.1s but not in Fire_CCI v5.1. Furthermore, the declining trend of the burned area since 2010 in Fire_CCI v5.1 but not in GFED4.1s may be attributed to the suppression of large fires (but not for small fires). Compared to the result of satellite data, model simulations produced a much larger estimate of burned area (7.54-16.91 × 10^4 km^2). Satellite-derived fire burned area proportion in China is comparable to the annual rate of 0.57% forest being burned in Canada, one of the fire-prone regions in the world (Stinson et al., 2011; Stocks et al., 2002). On the other hand, except for GFED4.1s that revealed a slightly increasing trend, other satellite products and model simulations suggested that burned area remained variable but without clear long-term trends. Multiple factors acted toward different directions in changing burned area. For example, land use and land cover changes in the recent decades tended to reduce burned area but CO_2 fertilization effect and other anthropogenic activities enhanced fire burnings (Fig. 8). The anomaly in burned area caused by any single driver appeared to have no trends within the study period.

In addition to the dynamics in the total burned area, the spatial distribution and seasonal timing of ecosystem fires are also strongly heterogeneous. For example, both satellite product and model simulations revealed high amounts of burning in Daxing'anling and South Yunnan (Fig. 3), regions dominated by boreal and subtropical dry forest, respectively. Numerous studies have suggested that these ecosystem types are typically fire-prone (Kasischke and Turetsky, 2006; Su et al., 2019; Van der Werf et al., 2008; Wilgen et al., 1985). The difference in fire seasonality between these two regions (Fig. 6) can be explained by climatic differences. The peak fire seasons in Daxing'anling are mainly late summer to early autumn, likely associated with a weakening monsoon (Cahoon et al., 1994). In subtropical Yunnan, where the climate pattern is characterized by the alternating wet and dry season as influenced by the shifting Indian oceanic warm current, fire peaks during the dry spring and winter (Zhang et al., 2013). Burning in East and South China and the Northeast Plain could be mostly attributed to prescribed agricultural fires.

Our results also revealed significant discrepancies between satellite-derived and simulated ecosystem fires. For instance, model simulations significantly overestimated burned area in eastern Qinghai-Tibetan Plateau (Fig. 3). This overestimation could be associated with the fire sensitivity to grassland cover by models. Briefly, the model estimates parameter values for fire spread (e.g., fuel load) in each grid cell as a weighted average of the values of different vegetation types, based on the fraction of each in the grid cell. Incorrect parameter values could have happened with the fuel load of grassland, where heavy grazing pressure might have significantly reduced available fuel, affecting fire occurrence and rate of spread. This grazing effect has not been incorporated in the model. Finally, factors other than grazing (such as biases in the input data or in ELM's gross primary productivity calculations) could also affect the model's simulation of biomass. While areas with more burned area simulated than observed might result from model

overestimation, the observational data themselves could also be negatively biased. The detection algorithm used by GFED4.1s is known to have a higher omission error in densely forested regions than in more open ecosystems (Giglio et al., 2009), which may explain the model-data disagreement in the dense forests of the boreal regions and South Yunnan (Fig. 3). Compared to the discrepancy in burned area between GFED4.1s and ELM model simulations, the discrepancy in fire carbon emissions was even larger (Table 1). Emissions in GFED4.1s were estimated based on both satellite data and a vegetation model. The large discrepancy may be attributed to ELM's overestimation of biomass compared to that used in GFED4.1s. Further model development and fine-tuning are required to reduce the uncertainty in estimating burned area and carbon emissions, and to improve our capacity in predicting China's ecosystem fire risks.

Fire induced carbon emissions during 1997–2016 were estimated as 23.02 TgC yr^{-1} by GFED4.1s. This GFED4.1s-estimated carbon emission was lower than the previous satellite-based estimates of Song et al. (2009) and Yan et al. (2006), but much higher than that derived from government statistics (Song et al., 2009; Yan et al., 2006; Lü et al., 2006), probably because government statistics typically only include large forest fires. Our semi-factorial simulations suggested strong impacts of anthropogenic factors on burned area and fire-induced carbon emissions (Fig. 8). Sound policy on fire management will be the key to help prevent devastating ecosystem fires, reduce the overall fire-induced carbon emission, and sustain ecosystem services.

Declaration Competing of Interest

The authors declare no conflict of interest.

Acknowledgements

Part of the funding was provided by the Carbon Mitigation Initiative (CMI) of the Princeton Environmental Institute, and by an Oak Ridge National Lab research subcontract to A.C. C. Y. and P. C. were supported by the fire_cci project (http://www.esa-fire-cci.org/) funded by the European Space Agency. S.R. was supported by a Graduate Research Fellowship from the U.S. National Science Foundation. R.T., J.M., X.S. and D.R. were supported by the Terrestrial Ecosystem Science Scientific Focus Area (TES SFA) project and the Reducing Uncertainties in Biogeochemical Interactions through Synthesis and Computing Scientific Focus Area (RUBISCO SFA) project funded by the US Department of Energy, Office of Science, Office of Biological and Environmental Research. Oak Ridge National Laboratory is supported by the Office of Science of the US Department of Energy under Contract No. DE-AC05-00OR22725.

Supplementary materials

Supplementary material associated with this article can be found, in the online version, at doi:10.1016/j.geosus.2020.03.002.

References

Abatzoglou, J.T., Williams, A.P., Boschetti, L., Zubkova, M., Kolden, C.A., 2018. Global patterns of interannual climate–fire relationships. Global Change Biol. 24 (11), 5164–5175.

Adab, H., Atabati, A., Oliveira, S., Gheshlagh, A.M., 2018. Assessing fire hazard potential and its main drivers in Mazandaran province, Iran: a data-driven approach. Environ. Monit. Assess. 190 (11), 670.

Archibald, S., Lehmann, C.E.R., Gómez-Dans, J.L., Bradstock, R.A., 2013. Defining pyromes and global syndromes of fire regimes. PNAS 110 (16), 6442–6447.

Archibald, S., Roy, D.P., van Wilgen, B.W., Scholes, R.J., 2009. What limits fire? An examination of drivers of burnt area in Southern Africa. Global Change Biol. 15 (3), 613–630.

Archibald, S., Scholes, R.J., Roy, D.P., Roberts, G., Boschetti, L., 2010. Southern African fire regimes as revealed by remote sensing. Int. J. Wildland Fire 19 (7), 861–878.

Barrett, K., McGuire, A.D., Hoy, E.E., Kasischke, E.S., 2011. Potential shifts in dominant forest cover in interior Alaska driven by variations in fire severity. Ecol. Applic. 21 (7), 2380–2396.

Beck, P.S.A., Goetz, S.J., Mack, M.C., Alexander, H.D., Jin, Y., Randerson, J.T., Loranty, M.M., 2011. The impacts and implications of an intensifying fire regime on Alaskan boreal forest composition and albedo. Global Change Biol. 17 (9), 2853–2866.

Bond-Lamberty, B., Peckham, S.D., Ahl, D.E., Gower, S.T., 2007. Fire as the dominant driver of central Canadian boreal forest carbon balance. Nature 450 (7166), 89–92.

Bowman, D.M.J.S., Balch, J.K., Artaxo, P., Bond, W.J., Carlson, J.M., Cochrane, M.A., D'Antonio, C.M., DeFries, R.S., Doyle, J.C., Harrison, S.P., Johnston, F.H., Keeley, J.E., Krawchuk, M.A., Kull, C.A., Marston, J.B., Moritz, M.A., Prentice, I.C., Roos, C.I., Scott, A.C., Swetnam, T.W., van der Werf, G.R., Pyne, S.J., 2009. Fire in the Earth System. Science 324 (5926), 481–484.

Cahoon, D.R., Stocks, B.J., Levine, J.S., Cofer, W.R., Pierson, J.M., 1994. Satellite analysis of the severe 1987 forest fires in northern China and southeastern Siberia. J. Geophys. Res. 99 (D9), 18627–18638.

Chen, D., Pereira, J.M., Masiero, A., Pirotti, F., 2017. Mapping fire regimes in China using MODIS active fire and burned area data. Appl. Geogr. 85, 14–26.

Chu, T., Guo, X., 2014. Remote sensing techniques in monitoring post-fire effects and patterns of forest recovery in boreal forest regions: A review. Remote Sens. 6 (1), 470–520.

Chuvieco, E., Lizundia-Loiola, J., Pettinari, M.L., Ramo, R., Padilla, M., Tansey, K., Mouillot, F., Laurent, P., Storm, T., Heil, A., Plummer, S., 2018. Generation and analysis of a new global burned area product based on MODIS 250 m reflectance bands and thermal anomalies. Earth Syst. Sci. Data 10 (4), 2015–2031.

Cochrane, M.A., Alencar, A., Schulze, M.D., Souza, C.M., Nepstad, D.C., Lefebvre, P., Davidson, E.A., 1999. Positive feedbacks in the fire dynamic of closed canopy tropical forests. Science 284 (5421), 1832–1835.

De Groot, W.J., Cantin, A.S., Flannigan, M.D., Soja, A.J., Gowman, L.M., Newbery, A., 2013. A comparison of Canadian and Russian boreal forest fire regimes. Forest Ecol. Manage. 294, 23–34.

Feurdean, A., Florescu, G., Vannière, B., Tanţău, I., O'Hara, R.B., Pfeiffer, M., Hickler, T., 2017. Fire has been an important driver of forest dynamics in the Carpathian Mountains during the Holocene. Forest Ecol. Manage. 389, 15–26.

Field, R.D., Van Der Werf, G.R., Fanin, T., Fetzer, E.J., Fuller, R., Jethva, H., Worden, H.M., 2016. Indonesian fire activity and smoke pollution in 2015 show persistent nonlinear sensitivity to El Niño-induced drought. Proc. Natl. Acad. Sci. 113 (3), 9204–9209.

Forbes, W.L., Mao, J., Jin, M., Kao, S., Fu, W., Shi, X., Riccuito, D.M., Thornton, P.E., Ribes, A., Wang, Y., Piao, S., Zhao, T., Schwalm, C.R., Hoffman, F.M., Fisher, J.B., Ito, A., Poulter, B., Fang, Y., Tian, H., Jain, A.K., Hayes, D.J., 2018. Contribution of Environmental Forcings to US Runoff Changes for the Period 1950-2010. Environ. Res. Lett. 13 (5), 054023.

Forbes, W.L., Mao, J., Ricciuto, D.M., Kao, S., Shi, X., Tavakoly, A.A., Jin, M., Guo, W., Zhao, T., Wang, Y., Thornton, P.E., Hoffman, F.M., 2019. Streamflow in the Columbia River Basin: Quantifying Changes Over the Period 1951-2008 and Determining the Drivers of Those Changes. Water Resour. Res. 55 (8), 6640–6652. doi:10.1088/1748-9326/aabb41.

French, N.H.F., de Groot, W.J., Jenkins, L.K., Rogers, B.M., Alvarado, E., Amiro, B., de Jong, B., Goetz, S., Hoy, E., Hyer, E., Keane, R., Law, B.E., McKenzie, D., McNulty, S.G., Ottmar, R., Pérez-Salicrup, D.R., Randerson, J., Robertson, K.M., Turetsky, M., 2011. Model comparisons for estimating carbon emissions from North American wildland fire. J. Geophys. Res.: Biogeosci. 116 (G4), G00K05.

Friedl, M.A., Sulla-Menashe, D., Tan, B., Schneider, A., Ramankutty, N., Sibley, A., Huang, X., 2010. MODIS Collection 5 global land cover: Algorithm refinements and characterization of new datasets. Remote Sens. Environ. 114 (1), 168–182.

Giglio, L., Loboda, T., Roy, D.P., Quayle, B., Justice, C.O., 2009. An active-fire based burned area mapping algorithm for the MODIS sensor. Remote Sens. Environ. 113 (2), 408–420.

Giglio, L., Randerson, J.T., van der Werf, G.R., 2013. Analysis of daily, monthly, and annual burned area using the fourth-generation global fire emissions database (GFED4). J. Geophys. Res.: Biogeosci. 118 (1), 317–328.

Giglio, L., Randerson, J.T., van der Werf, G.R., Kasibhatla, P.S., Collatz, G.J., Morton, D.C., DeFries, R.S., 2010. Assessing variability and long-term trends in burned area by merging multiple satellite fire products. Biogeosciences 7 (3), 1171–1186.

Guo, X.X., Li, X.H., Li, S.S., 2003. Characteristics of fire occurrences in the forests and grasslands of Inner Mongolia. Inner Mongolia Meteorol. 2003 (2), 28–30. (in Chinese)

Han, J., Shen, Z., Ying, L., Li, G., Chen, A., 2015. Early post-fire regeneration of a fire-prone subtropical mixed Yunnan pine forest in Southwest China: Effects of pre-fire vegetation, fire severity and topographic factors. For. Ecol. Manage. 356, 31–40.

Hantson, S., Arneth, A., Harrison, S.P., Kelley, D.I., Prentice, I.C., Rabin, S.S., Bachelet, D., 2016. The status and challenge of global fire modelling. Biogeosciences 13 (11), 3359–3375.

Hislop, S., Haywood, A., Jones, S., Soto-Berelov, M., Skidmore, A., Nguyen, T.H., 2020. A satellite data driven approach to monitoring and reporting fire disturbance and recovery across boreal and temperate forests. Int. J. Appl. Earth Observ. Geoinform. 87, 102034.

Hoffman, C.M., Sieg, C.H., Linn, R.R., Mell, W., Parsons, R.A., Ziegler, J.P., Hiers, J.K., 2018. Advancing the science of wildland fire dynamics using process-based models. Fire 1 (2), 32.

Hoffmann, W.A., Geiger, E.L., Gotsch, S.G., Rossatto, D.R., Silva, L.C., Lau, O.L., Haridasan, M., Franco, A.C., 2012. Ecological thresholds at the savanna-forest boundary: how plant traits, resources and fire govern the distribution of tropical biomes. Ecol. Lett. 15 (7), 759–768.

Hou, X., et al., 2019. 1:1 million vegetation map of China. National Tibetan Plateau Data Center. https://data.tpdc.ac.cn/en/(accessed 3 January 2020).

Huang, C., He, H.S., Liang, Y., Wu, Z., Hawbaker, T.J., Gong, P., Zhu, Z., 2018. Long-term effects of fire and harvest on carbon stocks of boreal forests in northeastern China. Ann. Forest Sci. 75 (2), 42.

Huntzinger, D.N., et al., 2013. The North American Carbon Program Multi-Scale Synthesis and Terrestrial Model Intercomparison Project - Part 1: Overview and experimental design. Geoscientific Model Dev. 6 (6), 2121–2133.
Kaiser, J.W., Heil, A., Andreae, M.O., Benedetti, A., Chubarova, N., Jones, L., Morcrette, J.-J., Razinger, M., Schultz, M.G., Suttie, M., van der Werf, G.R., 2012. Biomass burning emissions estimated with a global fire assimilation system based on observed fire radiative power. Biogeosciences 9 (1), 527–554.
Kantzas, E.P., Quegan, S., Lomas, M., 2015. Improving the representation of fire disturbance in dynamic vegetation models by assimilating satellite data: a case study over the Arctic. Geoscientific Model Dev. 8 (8), 2597–2609.
Kasischke, E.S., Turetsky, M.R., 2006. Recent changes in the fire regime across the North American boreal region—Spatial and temporal patterns of burning across Canada and Alaska. Geophys. Res. Lett. 33 (9) L09703.
Kaye, J., Romanyà, J., Vallejo, V., 2010. Plant and soil carbon accumulation following fire in Mediterranean woodlands in Spain. Oecologia 164 (2), 533–543.
Kloster, S., Mahowald, N.M., Randerson, J.T., Lawrence, P.J., 2012. The impacts of climate, land use, and demography on fires during the 21st century simulated by CLM-CN. Biogeosciences 9 (1), 509–525.
Knorr, W., Kaminski, T., Arneth, A., Weber, U., 2013. Impact of human population density on fire frequency at the global scale. Biogeosciences Discuss. 10, 15735–15778.
Knorr, W., Lehsten, V., Arneth, A., 2012. Determinants and predictability of global wildfire emissions. Atmos. Chem. Phys. 12 (15), 6845–6861.
Konovalov, I.B., Berezin, E.V., Ciais, P., Broquet, G., Beekmann, M., Hadji-Lazaro, J., Clerbaux, C., Andreae, M.O., Kaiser, J.W., Schulze, E.-D., 2014. Constraining CO2 emissions from open biomass burning by satellite observations of co-emitted species: a method and its application to wildfires in Siberia. Atmos. Chem. Phys. 14 (2), 3099–3168.
Kumar, S.S., Roy, D.P., 2018. Global operational land imager Landsat-8 reflectance-based active fire detection algorithm. Int. J. Digital Earth 11 (2), 154–178.
Le Page, Y., van der Werf, G.R., Morton, D.C., Pereira, J.M.C., 2010. Modeling fire-driven deforestation potential in Amazonia under current and projected climate conditions. J. Geophys. Res. 115, G03012.
Lehmann, C.E., Anderson, T.M., Sankaran, M., Higgins, S.I., Archibald, S., Hoffmann, W.A., Hutley, L.B., 2014. Savanna vegetation-fire-climate relationships differ among continents. Science 343 (6170), 548–552.
Li, F., Levis, S., Ward, D.S., 2013. Quantifying the role of fire in the Earth system – Part 1: Improved global fire modeling in the Community Earth System Model (CESM1). Biogeosciences 10 (4), 2293–2314.
Liu, Z., Ballantyne, A.P., Cooper, L.A., 2019. Biophysical feedback of global forest fires on surface temperature. Nat. Commun. 10 (1), 214.
Li, F., Zeng, X.D., Levis, S., 2012. A process-based fire parameterization of intermediate complexity in a Dynamic Global Vegetation Model. Biogeosciences 9 (7), 2761–2780.
Liu, G., Zhang, H., 2019. Temporal and spatial dynamic characteristics analysis of Inner Mongolia grassland fire. In: Risk Analysis Based on Data and Crisis Response Beyond Knowledge: Proceedings of the 7th International Conference on Risk Analysis and Crisis Response (RACR 2019). CRC Press, Athens, Greece, p. 125.
Lizundia-Loiola, J., Otón, G., Ramo, R., Chuvieco, E., 2020. A spatio-temporal active-fire clustering approach for global burned area mapping at 250 m from MODIS data. Remote Sens. Environ. 236, 111493 p.111493.
Lü, A., Tian, H., Liu, M., Liu, J., Melillo, J.M., 2006. Spatial and temporal patterns of carbon emissions from forest fires in China from 1950 to 2000. J. Geophys. Res. 111, D05313.
Malamud, B.D., Morein, G., Turcotte, D.L., 1998. Forest Fires: An Example of Self-Organized Critical Behavior. Science 281 (5384), 1840–1842.
Mao, J., Fu, W., Shi, X., Ricciuto, D.M., Fisher, J.B., Dickinson, R., Wei, Y., Shem, W., Piao, S., Wang, K., Rchwalm, R.C., Tian, H., Mu, M., Arain, A., Ciais, P., Cook, R., Dai, Y., Hayes, D., Hoffman, F.M., Huang, M., Huang, S., Huntzinger, D.N., Ito, A., Jain, A., King, A.W., Lei, H., Lu, C., Michalak, A.M., Parazoo, N., Peng, C., Peng, S., Poulter, B., Schaefer, K., Jafarov, E., Ehornton, P.E., Wang, W., Zeng, N., Zeng, Z., Zhao, F., Zhu, Q., Zhu, Z., 2015. Disentangling Climatic and Anthropogenic Controls on Global Terrestrial Evapotranspiration Trends. Environ. Res. Lett. 10 (9), 094008.
Metcalfe, D.B., Riccciuto, D., Palmroth, S., Campbell, C., Hurry, V., Mao, J., Keel, S.G., Linder, S., Shi, X., Nasholm, T., Ohlsson, K.E.A., Blackburn, M., Thornton, P.E., Oren, R., 2017. Informing Climate Models with Rapid Chamber Measurements of Forest Carbon Uptake. Global Change Biol. 23 (5), 2130–2139.
Miao, Y., Zhang, D., Cai, X., Li, F., Jin, H., Wang, Y., Liu, B., 2017. Holocene fire on the northeast Tibetan Plateau in relation to climate change and human activity. Quat. Internat. 443, 124–131.
Migliavacca, M., Dosio, A., Kloster, S., Ward, D.S., Camia, A., Houborg, R., Houston Durrant, T., Khabarov, N., Krasovskii, A.A., San Miguel–Ayanz, J., Cescatti, A., 2013. Modeling burned area in Europe with the Community Land Model. J. Geophys. Res.: Biogeosci. 118 (1), 265–279.
Mouillot, F., Schultz, M.G., Yue, C., Cadule, P., Tansey, K., Ciais, P., Chuvieco, E., 2014. Ten years of global burned area products from spaceborne remote sensing—A review: Analysis of user needs and recommendations for future developments. International J. Appl. Earth Observ. Geoinform. 26, 64–79.
Oliveira, S., Laneve, G., Fusilli, L., Eftychidis, G., Nunes, A., Lourenço, L., Sebastián-López, A., 2017. A common approach to foster prevention and recovery of forest fires in mediterranean Europe. Mediterranean Identities—Environment, Society, Culture. NHBS, Bonn, pp. 337–361.
Pausas, J.G., Fernández-Muñoz, S., 2012. Fire regime changes in the Western Mediterranean Basin: from fuel-limited to drought-driven fire regime. Climatic Change 110 (1–2), 215–226.
Pellegrini, A.F., Ahlström, A., Hobbie, S.E., Reich, P.B., Nieradzik, L.P., Staver, A.C., Jackson, R.B., 2018. Fire frequency drives decadal changes in soil carbon and nitrogen and ecosystem productivity. Nature 553 (7687), 194–198.
Prentice, I.C., Kelley, D.I., Foster, P.N., Friedlingstein, P., Harrison, S.P., Bartlein, P.J., 2011. Modeling fire and the terrestrial carbon balance. Global Biogeochem. Cycles 25 (3) GB3005.
Randerson, J.T., Chen, Y., van der Werf, G.R., Rogers, B.M., Morton, D.C., 2012. Global burned area and biomass burning emissions from small fires. J. Geophys. Res.: Biogeosci. 117, G04012.
[dataset], Randerson, J.T., van der Werf, G.R., Giglio, L., Collatz, G.J., Kasibhatla, P.S., 2017. Global Fire Emissions Database. ORNL DAAC, Oak Ridge, Tennessee, USA. Version 4.1 (GFEDv4).
Roy, D.P., Boschetti, L., 2009. Southern Africa Validation of the MODIS, L3JRC, and GlobCarbon Burned-Area Products. IEEE Trans. Geosci. Remote Sens. 47 (4), 1032–1044.
Sá, A.C., Benali, A., Fernandes, P.M., Pinto, R.M., Trigo, R.M., Salis, M., Pereira, J.M., 2017. Evaluating fire growth simulations using satellite active fire data. Remote Sens. Environ. 190, 302–317.
Shi, X., Thorton, P.E., Ricciuto, D.M., Hanson, P.J., Mao, J., Sebestyen, S., Griffiths, N., Bisht, G., 2015. Representing Northern Peatland Microtopography and Hydrology within the Community Land Model. Biogeosciences 12 (21), 6463–6477.
Shvidenko, A.Z., Shchepashchenko, D.G., Vaganov, E.A., Sukhinin, A.I., Maksyutov, S.S., McCallum, I., Lakyda, I.P., 2011. Impact of wildfire in Russia between 1998–2010 on ecosystems and the global carbon budget. Dokl. Earth Sci. 441 (2), 1678–1682.
Song, Y., Liu, B., Miao, W., Chang, D., Zhang, Y., 2009. Spatiotemporal variation in nonagricultural open fire emissions in China from 2000 to 2007. Global Biogeochem. Cycles 23, GB2008.
Staver, A.C., Archibald, S., Levin, S.A., 2011. The Global Extent and Determinants of Savanna and Forest as Alternative Biome States. Science 334 (6053), 230–232.
Stinson, G., Kurz, W.A., Smyth, C.E., Neilson, E.T., Dymond, C.C., Metsaranta, J.M., Boisvenue, C., Rampley, G.J., Li, Q., White, T.M., Blain, D., 2011. An inventory-based analysis of Canada's managed forest carbon dynamics, 1990 to 2008. Global Change Biol. 17 (6), 2227–2244.
Stocks, B.J., Mason, J.A., Todd, J.B., Bosch, E.M., Wotton, B.M., Amiro, B.D., Flannigan, M.D., Hirsch, K.G., Logan, K.A., Martell, D.L., Skinner, W.R., 2002. Large forest fires in Canada, 1959–1997. J. Geophys. Res.: Atmos. 107 (D1), 8149.
Su, Z., Tigabu, M., Cao, Q., Wang, G., Hu, H., Guo, F., 2019. Comparative analysis of spatial variation in forest fire drivers between boreal and subtropical ecosystems in China. Forest Ecol. Manage. 454, 117669.
Syphard, A.D., Keeley, J.E., Pfaff, A.H., Ferschweiler, K., 2017. Human presence diminishes the importance of climate in driving fire activity across the United States. Proc. Natl. Acad. Sci. U.S.A. 114 (52), 13750–13755.
Tao, Y., Di, X., Jin, S., 2013. Research on temporal and spatial distribution of forest fire in China. World Forest. Res. 26 (5), 75–80. (in Chinese)
Tian, X., Shu, L., Zhao, F., Wang, M., McRae, D.J., 2011. Future impacts of climate change on forest fire danger in northeastern China. J. Forest. Res. 22 (3), 437–446.
Van Den Hurk, B., et al., 2016. "LS3MIP (v1.0) Contribution to CMIP6: The Land Surface, Snow and Soil Moisture Model Intercomparison Project - Aims, Setup and Expected Outcome. Geoscientific Model Dev. 9 (8), 2809–2832.
Van der Werf, G.R., Randerson, J.T., Giglio, L., Collatz, G.J., Kasibhatla, P.S., Arellano Jr., A.F., 2006. Interannual variability in global biomass burning emissions from 1997 to 2004. Atmos. Chem. Phys. 6 (11), 3423–3441.
Van der Werf, G.R., Randerson, J.T., Giglio, L., Collatz, G.J., Mu, M., Kasibhatla, P.S., Morton, D.C., DeFries, R.S., Jin, Y., van Leeuwen, T.T., 2010. Global fire emissions and the contribution of deforestation, savanna, forest, agricultural, and peat fires (1997–2009). Atmos. Chem. Phys. 10 (23), 11707–11735.
Van der Werf, G.R., Randerson, J.T., Giglio, L., Gobron, N., Dolman, A.J., 2008. Climate controls on the variability of fires in the tropics and subtropics. Global Biogeochem. Cycles 22 (3), GB3028.
Van der Werf, G.R., Randerson, J.T., Giglio, L., Van Leeuwen, T.T., Chen, Y., Rogers, B.M., Yokelson, R.J., 2017. Global fire emissions estimates during 1997-2016. Earth Syst. Sci. Data 9 (2), 697–720.
Veraverbeke, S., Rogers, B.M., Randerson, J.T., 2015. Daily burned area and carbon emissions from boreal fires in Alaska. Biogeosciences 12 (11), 3579–3601.
Wang, C., Gower, S.T., Wang, Y., Zhao, H., Yan, P., Bond-Lamberty, B.P., 2001. The influence of fire on carbon distribution and net primary production of boreal Larix gmelinii forests in north-eastern China. Global Change Biol. 7 (6), 719–730.
Weise, D.R., Fletcher, T.H., Mahalingam, S., Zhou, X., Sun, L., 2017. Fire spread in chaparral: comparison of data with flame-mass loss relationships. In: Proceedings 8th International Symposium on Scale Modeling, p. 333, Sep. 12-14, 2017, Portland, OR.
Wilgen, B.W.V., Maitre, D.C.L., Kruger, F.J., 1985. Fire Behaviour in South African Fynbos (Macchia) Vegetation and Predictions from Rothermel's Fire Model. J. Appl. Ecol. 22 (1), 207–216.
Williams, R.J., Cook, G.D., Gill, A.M., Moore, P.H.R., 2009. Fire regime, fire intensity and tree survival in a tropical savanna in northern Australia. Austr. J. Ecol. 24 (1), 50–59.
Wirth, C., Lichstein, J.W., Dushoff, J., Chen, A., Chapin, F.S., 2008. White spruce meets black spruce: dispersal, postfire establishment, and growth in a warming climate. Ecol. Monogr. 78 (4), 489–505.
Wooster, M.J., Zhukov, B., Oertel, D., 2003. Fire radiative energy for quantitative study of biomass burning: derivation from the BIRD experimental satellite and comparison to MODIS fire products. Remote Sens. Environ. 86 (1), 83–107.
Yang, X., Thornton, P.E., Ricciuto, D.M., Post, W.M., 2014b. The Role of Phosphorus Dynamics in Tropical Forests - A Modeling Study Using CLM-CNP. Biogeosciences 11 (6), 1667–1681.
Yan, X., Ohara, T., Akimoto, H., 2006. Bottom-up estimate of biomass burning in mainland. China. Atmos. Environ. 40 (27), 5262–5273.
Yang, J., Tian, H., Tao, B., Ren, W., Kush, J., Liu, Y., Wang, Y., 2014a. Spatial and temporal patterns of global burned area in response to anthropogenic and environmental factors: Reconstructing global fire history for the 20th and early 21st centuries. J. Geophys. Res.: Biogeosci. 119 (3), 249–263.

Ying, L., Han, J., Du, Y., Shen, Z., 2018. Forest fire characteristics in China: Spatial patterns and determinants with thresholds. Forest Ecol. Manage. 424, 345–354.
Yuan, F., Yi, S., McGuire, A.D., Johnson, K.D., Liang, J., Harden, J., Kasischke, E.S., Kurz, W., 2012. Assessment of Historical Boreal Forest C Dynamics in Yukon River Basin: Relative Roles of Warming and Fire Regime Change. Ecol. Applic. 22 (8), 2091–2109.
Yue, C., Ciais, P., Cadule, P., Thonicke, K., Archibald, S., Poulter, B., Hao, W.M., Hantson, S., Mouillot, F., Friedlingstein, P., Maignan, F., Viovy, N., 2014. Modelling fires in the terrestrial carbon balance by incorporating SPITFIRE into the global vegetation model ORCHIDEE – Part 1: Simulating historical global burned area and fire regime. Geosci. Model Dev. Discuss. 7 (6), 2377–2427.
Zeng, Z.Z., Chen, A.P., Piao, S.L., Rabin, S., Shen, Z.H., 2014. Environmental determinants of tropical forest and savanna distribution: A quantitative model evaluation and its implication. J. Geophys. Res.: Biogeosci. 119 (7), 1432–1445.
Zhang, M., He, J., Wang, B., Wang, S., Li, S., Liu, W., Ma, X., 2013. Extreme drought changes in Southwest China from 1960 to 2009. J. Geogr. Sci. 23 (1), 3–16.
Zhang, Y., Shen, L., Ren, Y., Wang, J., Liu, Z., Yan, H., 2019. How fire safety management attended during the urbanization process in China? J. Cleaner Prod. 236, 117686.
Zhao, M., Running, S.W., 2010. Drought-Induced Reduction in Global Terrestrial Net Primary Production from 2000 Through 2009. Science 329 (6062), 940–943.
Zhong, M., Fan, W., Liu, T., Li, P., 2003. Statistical analysis on current status of China forest fire safety. Fire Saf. J. 38 (3), 257–269.